Atmos. Chem. Phys. Discuss., 6, 9389–9429, 2006
www.atmos-chem-phys-discuss.net/6/9389/2006/

Atmospheric Chemistry and Physics Discussions

An annual cycle of long lived stratospheric gases from MIPAS

M. N. Juckes

British Atmospheric Data Centre, SSTD, Rutherford Appleton Laboratory, Chilton, Didcot, Oxfordshire, OX11 0QX, UK

Received: 20 July 2006 – Accepted: 9 September 2006 – Published: 26 September 2006

Correspondence to: M. N. Juckes (m.n.juckes@rl.ac.uk)

Abstract

MIPAS, on ENVISAT, has made high quality observations of ozone, methane and water vapour. Gridded fields, at 4 hourly intervals and approximately 2 degree resolution, have been calculated for all of 2003 using data assimilation with isentropic advection as a constraint. The gridded fields are validated against independent measurements (from 7 other instruments in the case of ozone, 3 for water vapour and one for methane). For ozone the results are in agreement with previously published results. For water vapour the bias relative to HALOE is below 10% between 20 and 48 km, and the standard error is below 12% in this range. Departures from SAGE II and POAM III are substantially larger. The methane analysis has a bias of less than 5% relative to HALOE between 23 and 40 km, with a standard error less than 10% in this height range. The water vapour field clearly reflects the upward motion in the lower tropical stratosphere, while both water vapour and methane show the signature of advection higher up. In the polar regions the descent in the vortex is clearly visible, with strong descent in autumn giving way to weaker descent through the winter. Descent rates of around 100 m/day are found during the formation of the polar vortices, slowing to around 30 m/day during the winter. Ascent of around 20 m/day in the tropics is revealed by the water vapour and total observed hydrogen fields (4 times the methane plus twice the water vapour concentration). The total observed hydrogen is depleted where air is advected down from the upper mesosphere.

1 Introduction

Stratospheric water vapour and methane are important greenhouse gases. Methane has been increasing steadily due to anthropogenic emissions. Water vapour is also increasing, in part due to oxidation of the increasing methane content (e.g. Rosenlof et al., 2001; Rind and Lonergan, 1995; Shindell, 2001)

The Michelson Interferometer for Passive Atmospheric Sounding (MIPAS) instrument

ACPD

6, 9389–9429, 2006

on the ENVISAT[1] (Fischer and Oelhaf, 1996; Tsidu et al., 2003; Glatthor et al., 2005) was operational for 20 months. The central 12 month period (January to December 2003) had near continuous global coverage. This gives unprecedented resolution of the day to day evolution of these key gases.

This paper presents assimilated fields of ozone, methane and water vapour. The assimilation algorithm is exactly as described in Juckes (2006) (hereafter J2006). Isentropic advection is used as a constraint. No account is taken of vertical structure: the analysis is carried out independently on each of 15 isentropic surfaces.

Assimilation of MIPAS ozone data has been discussed in Geer et al. (2006) and J2006. Here, new results for methane and water vapour are introduced. These two gases are important in their own right as significant players in the radiation budget (e.g. Shine, 1993), but also serve to illustrate the stratospheric circulation. The role of the polar vortex as a distinct air mass with special chemical properties has been a matter of special interest since the development of the Antarctic polar ozone hole (Farman et al., 1985; Solomon et al., 2005). The observation track of MIPAS crosses the pole every orbit, giving exceptional coverage of this key region of the stratosphere.

The next section summarises the methods used. Section 3 then describes the validation against independent measurements. Section 4 looks at the annual cycle in the 3 assimilated species. Section 5 looks at the evolution on shorter time scales, showing how the assimilated fields faithfully track a strong disturbance to the polar vortex. Section 6 looks at equivalent zonal means and introduces the total observed hydrogen.

2 Methodology and data

The MIPAS level 2 offline product (ESA, 2004) was used, versions 4.59 (2772 profiles), 4.61 (213 284) and 4.62 (25 328). The offline product has been found to be significantly

[1]The European Space Agency's "Environmental Satellite", launched on Friday 1 March 2002.

improved over the near-real time product (e.g. Fonteyn et al., 2004). The fields are interpolated onto isentropic surfaces prior to assimilation using the MIPAS retrieved temperature profiles and linear interpolation with respect to potential temperature.

The assimilation uses meteorological fields from the European Centre for Medium-Range Weather Forecasts (ECMWF) operational analyses.

As in J2006, the assimilation is run in overlapping 50 day blocks, with each block being computed as the minimisation of a single cost function:

$$\mathcal{J} = \sum_i \sigma_{\mathrm{obs}:i}^{-2} \left[\chi_{\mathrm{obs}:i} - \chi(\lambda_{\mathrm{obs}:i}, \phi_{\mathrm{obs}:i}, t_{\mathrm{obs}:i}) \right]^2 + \int\int \left\{ w_{\mathrm{ap}} \left[\chi_t + \mathbf{u} \cdot \nabla \chi \right]^2 + w_{\mathrm{num}} \left| \left(c_1 \frac{\partial}{\partial t}, \nabla \right) \left(c_1^2 \frac{\partial^2 \chi}{\partial t^2} + \nabla^2 \chi \right) \right|^2 \right\} dA dt \quad (1)$$

where χ is the tracer mixing ratio in units of ppmv (parts per million by volume), λ, ϕ, t are longitude, latitude and time respectively, $\mathbf{u}$ is the horizontal wind velocity, $\sigma_{\mathrm{obs:i}}^2$ is the observation error variance, with the subscript i here and elsewhere labeling the observation. Constants used here are c_1=0.5 days per radian =.0068s m^{-1}, w_{ap}=50 day^2 ppmv^{-2}=3.7×10^{11}s^2 ppmv^{-2}, and w_{num}=1.45×10^{-6}radian^6 ppmv^{-2}=9.7×10^{34}m^6 ppmv^{-2}. The summation is over all observations, and the integrations are over the sphere ($dA = \cos\phi d\lambda d\phi$) and over an assimilation window of around 50 days. The large value of the w_{num} in SI units reflects scale-selectivity, which ensures the solution is well behaved on the grid scale. There are no prescribed error covariance structures in this formulation: the variational problem is completely defined by the constants quoted above and the observational data ($\chi_{\mathrm{obs:i}}$, $\sigma_{\mathrm{obs:i}}$, i=1, N_{obs}, where N_{obs} is the number of observations).

The solution is found by solving $\mathcal{A}[\chi]$=0, where $\mathcal{A}$ is differential operator resulting from the first variation of Eq. (1) wrt. χ (see J2006).

ACPD
6, 9389–9429, 2006

The spatial and temporal discretisation used here are 1.875 degrees and 4 h respectively, with longitudinal thinning of the grid towards the pole as described in J2006. The analysis period is split into 12 monthly assimilation windows, each extending around 50 days from the 21st of the previous month through to the 10th of the subsequent month. Two exceptions to this rule are the January window, which starts on 1 January, and the December window, which ends on 31 December. As described in J2006, the analysis from the ends of each assimilation window (with the exception of the start of January and end of December) is discarded.

3 Validation

Validation data was employed from the following instruments (with level 2 data version in square brackets): Solar Backscatter Ultraviolet (SBUV; Planet et al., 2001) [61610], Stratospheric Aerosol and Gas Experiment (SAGE II and III; Thomason and Taha, 2003) [6.2], Polar Ozone and Aerosol Measurement (POAM III; Lumpe et al., 2003; Pierce et al., 2003) [3], Optical Spectrograph and Infrared Imaging System (OSIRIS; von Savigny et al., 2003) [1.2], and Halogen Occultation Experiment (HALOE; Brühl et al., 1996) [19].

In addition ozonesonde data, provided by the World Ozone and Ultraviolet Radiation Data Centre (WOUDC) [2], from 38 stations, listed in the appendix of J2006, was used.

J2006 validated 6 months of ozone data. Here, that analysis has been extended to 12 months. The results for ozone do not differ significantly from those reported earlier. Figure 1 shows a summary of the ozone validation against independent observations on the 850 K isentropic surface. The assimilated MIPAS field shows no significant drift relative to SBUV, HALOE, SAGE II or SAGE III. There is a slight shift relative to POAM

[2] WOUDC is one of five World Data Centres which are part of the Global Atmosphere Watch programme of the World Meteorological Organization. The WOUDC is operated by the Experimental Studies Division of the Meteorological Service of Canada (web address: http://www.woudc.org).

in November and December, but this shift is not reproduced against other instruments. The mean difference from the sonde data shows more variability, but this does not appear to be systematic (it should be noted that this level (850 K) is towards the upper limit of the sondes' range). Overall, the majority of comparisons support the view that bias in the MIPAS is small and without systematic drift.

Figure 2 shows the same diagnostics for the water vapour fields. There is no significant drift against HALOE and SAGE II, but, as with ozone, there is a drift relative to POAM III. The agreement between HALOE, MIPAS and SAGE II suggests that POAM III is at fault here. There is, however, a jump at the start of August which is present in both the POAM and SAGE II differences. This needs to be allowed for in physical interpretation of the analyses below.

For methane (Fig. 3) there is only one validation instrument, HALOE. The mean differences increase slightly through the year, ending with HALOE reading 0.05 ppmv lower than the MIPAS assimilation.

In Figs. 1–3 the orange curve shows the mean and standard error of the MIPAS observations minus analysis. The mean is very close to zero in all cases, as expected from the construction of the analysis (J2006). In water vapour there is a significant increase in the standard deviations both in June and July and again in November and December, whereas the standard deviations for ozone and methane remain relatively steady through the year. This suggests there is some anomalous behaviour in the water vapour retrievals in the months mentioned above. During these periods the assimilation has a lower standard deviation relative to the independent HALOE data than it does relative to the observations used as input.

Figure 4 shows vertical profiles of the isentropic mean of the observations minus analysis for the ozone data. The structure over the 12 month period studied here is essentially the same as the 6 month period analysed in J2006. Mean differences are low between 500 and 1250 K (i.e. approximately from 20 to 40 km – heights of isentropic surfaces can be read from Fig. 7 below). Above and below that range it appears that MIPAS is measuring low (as described in J2006, the present analysis is

unbiased relative to the observations which are used to generate it).

The water vapour mean and standard error profiles (Fig. 5) suggest a slight positive bias in MIPAS in the upper stratosphere.

As with the 850 K time series shown in Fig. 2, the standard error of the difference between the HALOE measurements and the assimilation is less at one level (1250 K) than the standard error of the difference between the assimilation and the observations which were used to create it (this is not the case for the root-mean-square difference). This suggests that the assimilation of the data is reducing the random error present in the input data. In terms of the standard deviation, the agreement with HALOE is substantially better than that with POAM III at all levels and better than that with SAGE II above 500 K. Between 500 K and 850 K the bias relative to POAM III is very small (around 2%), but there are larger biases relative to SAGE II and POAM III.

Figure 6 shows profiles of mean anomaly and standard error of the methane analyses relative to HALOE observations. There is a positive relative bias in the analyses at all heights, less than 5% between 600 K and 1700 K. The standard error is under 10% over this height range.

For both water vapour and methane, Figs. 5 and 6 also show results of a nearest neighbour comparison between the MIPAS profiles used as input for the assimilations and the validating data. The mean differences are very similar to those found with the assimilated data, but the standard errors are larger in the nearest neighbour comparisons.

All the validation data (in the form of differences between analyses and validating observations) are supplied as netcdf files in the supplementary material (http://www.atmos-chem-phys-discuss.net/6/9389/2006/acpd-6-9389-2006-supplement.zip).

4 Annual cycle

The annual cycle of methane and water vapour has been discussed by Randel et al. (1998); Dunkerton (2001), using HALOE data. The evolution of the present data

through the year reproduces the main features highlighted in previous studies. Figure 7 shows time-height sections of ozone, water vapour and methane, averaged over 3 equivalent latitude bands. Averaging around equivalent latitude bands[3] results in greater continuity because the averaging volume follows the short period dynamical displacements of the airmass. A 9 day period at the end of May during which there are no MIPAS observations is blanked out of the plots.

The zonal mean water vapour in the tropics (Fig. 7f) shows a very clear "tape recorder" signal (Mote et al., 1996): that is, a pattern imprinted on the air at the tropopause is carried upwards in the rising branch of the Brewer-Dobson circulation, rising at around 20 m/day (the slope of the red arrow in Fig. 7f). The tape-recorder signal is not visible in the methane fields (Fig. 7g). In the mid and upper stratosphere, in contrast, the methane and water vapour isolines follow each other closely, being displaced upwards in September to January, and downwards in March to July. This reflects the fact that the anomalies in this region are controlled by a balance between advection and chemical relaxation (Dunkerton, 2001), so that the structure in the anomalies represents the variation in the upward advection. In the lower stratosphere the chemical relaxation is slower and the anomalies reflect the air mass history.

The polar regions show a larger annual cycle and greater short term variability, primarily in the winter months. The evolution of the temperature structure is shown in Fig. 8. In the lower stratosphere, southern hemisphere, the coldest temperatures are reached towards the end of July. At 40 km, by contrast, the coldest temperatures occur just after the equinox. The onset of gradual warming after that date coincides with an increase in variability (Fig. 9). At the end of the winter there is a sharp rise in the pressure, such that there is, somewhat counter-intuitively, a sudden drop in potential temperature towards the end of the winter (this shows up as a step in the green isentropes in Fig. 8a and the corresponding frames of Fig. 7). The winter season in the

[3]The equivalent latitude, ϕ_{equiv}, is defined to be constant on contours of Ertel's potential vorticity, PV, and valued such that the total area over which $PV > PV_0$ is given by $4\pi \left\{1. - \cos\left[\phi_{\text{equiv}}(PV_0)\right]\right\}$.

northern hemisphere is not illustrated as clearly here because the study period only includes the end of one winter and the start of the next. It is, however, clear that the seasonal minimum in the upper stratosphere is, similarly, shortly after the equinox. In the lower stratosphere the high frequency variability sets in earlier.

Returning to the tracer fields shown in Fig. 7. In Fig. 7a we see the onset of chemical ozone loss in late September (Farman et al., 1985; Crutzen and Arnold, 1986; Crutzen and Lelieveld, 2001) in the southern vortex. Geer et al. (2006) show that MIPAS underestimates the extent of this loss, but it is nevertheless clearly distinguishable from the midwinter maximum in ozone seen in the northern hemisphere. The ozone loss is preceded by drying out of the lower stratosphere in late June (Fig. 7d).

In the mid stratosphere, the polar methane shows strong descent in the late summer and autumn followed by weaker descent throughout the winter. The overall pattern is as reported by Randel et al. (1998), but the present data resolve this with better temporal resolution than HALOE and it is possible to see marked switch in behaviour between the autumn and winter regimes. In the upper stratosphere there is a pronounced minimum, in both hemispheres, around the equinox at the start of the winter season, with mean values falling below 0.1 ppmv. This coincides with the onset of variability and the temperature minimum seen in Figs. 8, 9. This suggests that the initial minimum is the result of air descending from the mesosphere without mixing. Inspection of potential vorticity fields from the ECMWF analyses (not shown) support the interpretation that the subsequent increase is due to horizontal mixing by planetary scale disturbances. A number of authors have looked at early winter warmings in the mid-stratosphere (see Scott and Haynes, 2002), but this mixing, which is occurring earlier and higher, does not appear to have been investigated.

In March to May the descent rate at 30 km is around 100 m/day (the slope of the red arrows in Fig. 7). This descent is visible both in the methane and water vapour fields. At this level, the descent is weak in June and July but becomes strong again in August to October. The overlay of the potential temperature contours shows that the spring descent is a different dynamical process to that occurring in the autumn.

In the autumn the air mass is clearly crossing the isentropes, whereas in the spring the isentropes are also descending at a significant rate. Unlike the radiative cooling in autumn, which caused isentropes to rise and material contours to sink, the spring is a time of dynamically forced descent, carrying both isentropes and material contours downwards. [4]

Engel et al. (2006) observe a layer of mesospheric air descending from 30 km in late January to 25 km in early March 2003, and report a modelling study which shows this air descended during the previous autumn. This is highly consistent with the picture shown in Figs. 7e, h (lower left red arrow), where a tongue of low methane, high water vapour air persists and descend at a time when the layers higher in the stratosphere are returning to more typical stratospheric values. A similar pattern is seen in Fig. 7g (lower right red arrow), suggesting that this phenomenon is a recurring one. The pattern is not so clear in the southern hemisphere water vapour.

The methane fields in both hemispheres suggest that there has been descent of around 20 km through the year, bringing air down from 40 km to 20 km while preserving its chemical composition. This compares with an estimate of 13 km made by Rex et al. (1999) based on a comparison between air inside and outside the vortex.

The water vapour shows a similar pattern, with the noticeable exception of anomalous loss in the southern winter as the vapour freezes out (e.g. Benson et al., 2006). Also note that the sharp drop in mid-stratospheric water vapour a the start of August in Fig. 7d is not reflected by any similar change in the methane (Fig. 7g) but does coincide with a jump in the validation biases (Fig. 2), so that a discontinuity in measurement characteristics is the most likely explanation of this feature. This anomaly aside, the pattern of descent is consistent with that calculated by Rosenfield et al. (1994).

[4] Such dynamically forced descent occurring below the level of evidence of "downward control" (Haynes et al., 1991), but the papers presenting this idea fail to distinguish between diagnostic determination and causal determination.

ACPD
6, 9389–9429, 2006

5 Meteorology

5.1 Advection versus chemistry

The equivalent latitude means give a useful overview of the annual cycle. This section looks at variability on shorter timescales. Figure 10 shows the analysed tracer fields during a break up of the northern polar vortex. The corresponding flow field is illustrated using the potential vorticity in Fig. 11. The vortex is displaced form the pole and splits into two halves while an anticyclonic circulation is established over the pole. The ozone field at first mirrors the potential vorticity field, with the low ozone in the vortex core being advected around in the disturbed vortex. On 19 April, however, a new low centre appears in a region of low potential vorticity. The dynamical anomaly is a response to rapid meridional transport and does not show any obvious influence of diabatic processes. At this level ozone is subject to significant chemical evolution, and the ozone advected into the polar night is being destroyed. The assimilation code used here does not have any explicit representation of chemistry but the consequences of the chemistry are nevertheless present in the analysis through the observations.

The methane and water vapour fields (Figs. 10e–l) also show the break up of the vortex, but unlike the ozone field we see no evidence of chemistry. In the previous section it was noted that the chemistry of these species in the upper stratosphere starts to compete with vertical advection, but the faster horizontal advection can still be viewed as nearly conservative.

The analysis clearly shows the preservation of air mass properties as the vortex breaks up. It was shown in J2006 that the typical information retention time of the analysis was around 2 days. Beyond this time information from earlier observation is replaced by new observations. Thus, continuity of air mass properties for longer time scales must reflect continuity in the observations.

ACPD
6, 9389–9429, 2006

6 Equivalent zonal means

We now look at latitude-height sections of fields averaged at constant equivalent latitude, referred to here as equivalent zonal means (Figs. 12 and 13). Similar structures are visible in the simple zonal mean fields, but some of the detail is lost or blurred.

The equivalent zonal mean water vapour (panels a, b and c in Figs. 12 and 13) shows many of the features described in Sect. 4 from a different perspective. The tape recorder is seen as an isolated patch of relatively dry air. As noted in Sect. 4, the shapes of the methane isopleths (panels d, e and f in Figs. 12 and 13) differ from those of the water vapour in the lower tropical stratosphere, but there is a change in behaviour in the upper stratosphere where both methane and water vapour isopleths reflect a competition between vertical advection and chemical change.

Both the water vapour and the methane fields show a strong contrast between the tropical region and the sub-tropics. The tropical band is characterised by air advected up from the tropopause. The air in sub-tropics is, with respect to the time since it was in the troposphere, older.

6.1 Total observed hydrogen

The main reaction affecting water vapour and methane in the stratosphere is the gradual photolysis of methane to water vapour. This reaction leaves the quantity "total observed hydrogen" (H_{TO}) constant:

$$H_{TO} \stackrel{\text{def}}{=} 2[H_2O] + 4[CH_4]. \quad (2)$$

Molecular hydrogen is also thought to be a significant component of the total hydrogen budget in the mesosphere, but is not included in the observations used here. Previous studies have found H_{TO} to be nearly constant with height. The last column in Figs. 12, 13 displays the zonal mean H_{TO}. We see a tape-recorder signal is resolved, and there is a large (relative to the variability in the rest of the field) positive anomaly in the upper stratosphere.

ACPD
6, 9389–9429, 2006

In both the winter poles there is a strong low anomaly in the mesosphere where there is known to be downwards advection. This may be due to photo-dissociation of water vapour in the upper mesosphere into hydrogen and oxygen. As the air is advected down the hydrogen would be oxidized back to water vapour, explaining the recovery of H_{TO}. This is consistent with the findings of Harries et al. (1996) who attribute it to downward advection of mesospheric air with a higher molecular hydrogen content.

The large band of positive anomalies across the upper stratosphere remains as an unexplained structure. It is possible that this is due do observational error. An alternative would be that there is another source of hydrogen atoms, such as cometary material entering the atmosphere. These two possibilities will be discussed further below. Figure 14 shows H_{TO} fields corresponding to the water vapour and methane fields of Fig. 7. In Fig. 14c the "tape-recorder" signal is clearly visible. At the poles, however, the fields to not show the clear patterns of downwards advection seen in the water vapour and methane fields. In the northern hemisphere there is some indication of a positive anomaly at around 25 km in January and in December which might be indicative of enhanced hydrogen content being advected downwards.

Nassar et al. (2005) present data from the ACE-FTS instrument for February to April 2004. They show a fall in H_{TO} (presented as "equivalent water" which is exactly half H_{TO}) above 60 km, averaged over 30 N to 66 N. Here we see that the reduced H_{TO} concentrations extend to lower heights at high winter latitudes. Figure 1 of Nassar et al. (2005) also shows a weak peak in H_{TO} between 50 and 60 km, however, the amplitude is less than the error bars and the altitude is higher than the peak found here (around 40 km at that time and latitude, albeit for a different year).

It was noted above that the methane and water vapour fields show strong gradients between the tropics and sub-tropics. The H_{TO} field, on the other hand, shows anomalies spreading out to near global extent. They do not, however, spread out along isentropes. This structure could result from the competition between meridional transport and shearing by vertical advection.

The generally high values of H_{TO} in the upper stratosphere are not are not seen in the HALOE data. One explanation is that the bias between HALOE and MIPAS water vapour fields at these heights reflects an error in MIPAS. However, Hannegan et al. (1998) have suggested that there is a significant source (of the order or 2 Tg/year) of water vapour in the upper atmosphere from cometary material. This would be advected into the stratosphere in the form of H_2 and then mixed out. Some support for the latter theory is seen in the high values which persist into the mid-stratosphere of the polar vortex. Figure 15 illustrate how high H_{TO} values coincide with the centre of the vortex and very low ozone values (2.75 ppmv). The persistence of the high H_{TO} into the core of the winter vortex, where it would be advected by the meridional circulation, suggests that there is some truth in the high values. Figures 16 shows an equivalent snapshot in the southern hemisphere. The H_{TO} field is noisier here. There is again a contrast between the tropics and high latitudes, but here the change takes place mainly across the sub-tropical barrier, not across the vortex boundary.

However, there is an alternative explanation for the apparent material advection of excess H_{TO}. Geer et al. (2006) show that MIPAS ozone fields have a positive bias in the centre of the ozone hole: the retrieval is unable to reproduce the near zero values measured there by sondes and by HALOE. The values of methane in the centre of the vortex are also extremely small (Figs. 15, 16), following oxidation to water vapour in the mesosphere. It is possible that the retrieval is, as with ozone, introducing a small positive bias in these circumstances. Such a bias would be co-located with the low methane values and so would appear to be advected conservatively.

This explanation does not, however, fully explain the southern hemisphere view. Here there is an extended area of excess H_{TO} bounded by the sub-tropical transport barrier. The signal is noisier, but it is no longer coincident with extreme low methane values.

ACPD
6, 9389–9429, 2006

7 Conclusions

The MIPAS ozone, water vapour and methane fields have been used to construct gridded fields for the whole of 2003. Comparison with independent observations shows good agreement: for ozone the mean bias relative to other instruments is generally less than 5% in amplitude up to 1250 K. Above that height the ozone analyses appear to have a negative bias, though the agreement with HALOE remains good up to 2000 K. The random error is generally between 5 and 10%, agreement with HALOE being best above 1000 K and agreement with SAGE II & III being best below this level. In water vapour the analyses generally have a high bias of 5 to 10%, up to 2400 K. Random errors relative to HALOE are as low as 5% in the lower stratosphere, but larger relative to other instruments and relative to HALOE in the upper stratosphere. For methane, the analyses are high relative to HALOE, though this bias is less than 5% through much of the stratosphere. The random error grows from around 7% at 500 K to 20% at 3000 K.

In combination, the analyses of the 3 gases provide a rich record of transport processes through the year in the stratosphere. In the tropics, both water vapour and "observed total hydrogen" (H_{TO}, defined here as the hydrogen content of the observed methane and water vapour) fields show a clear "tape recorder" signal, indicating an ascent rate in the tropical lower stratosphere of around 20 m/day.

At high latitudes, both water vapour and methane show a deep region of descent within the polar vortex, with a rate of around 100 m/day. In the course of the winter air from the mesosphere descends to below 20 km.

In the winter mesosphere the H_{TO} values are depleted, as found by Harries et al. (1996), who conclude that water vapour has been photolysed to molecular hydrogen.

Between 40 and 50 km there is a band of enhanced H_{TO} values in the analyses. This could result from enhanced hydrogen content in the mesosphere, produced by deposition of cometary material in the atmosphere, being advected down and then oxidised to become observable in the upper stratosphere. However, the evidence is patchy and the anomaly may be due to instrumental biases. To explain the measurements any

ACPD
6, 9389–9429, 2006

EGU

such error must have the property of being conserved following the mesospheric air mass as it descends in the nascent stratospheric polar vortices. A (hypothetical) bias associated with extremely low methane would satisfy this condition.

Acknowledgements. This work was funded by NERC through BADC. I am grateful for all the data used in this study, which was of high quality and provided freely from the sources cited. I would like to thank A. Dhudhia and C. Piccolo for help with the MIPAS data.

References

Benson, C. M., Drdla, K., Nedoluha, G. E., Shettle, E. P., Hoppel, K. W., and Bevilacqua, R. M.: Microphysical modeling of southern polar dehydration during the 1998 winter and comparison with POAM III observations, J. Geophys. Res., 111, D07201, doi:10.1029/2005JD006506, 2006. 9398

Brühl, C., Drayson, S. R., II, J. M. R., Crutzen, P. J., McInerney, J. M., Purcell, P. N., Claude, H., Gernandt, H., McGee, T. J., McDermid, I. S., and Gunson, M. R.: Halogen occultation experiment ozone channel validation, J. Geophys. Res., 101, 10 217–10 240, 1996. 9393

Crutzen, P. and Arnold, F.: Nitric-acid cloud formation in the cold antarctic stratosphere – a major cause for the springtime ozone hole, Nature, 324, 651–655, 1986. 9397

Crutzen, P. and Lelieveld, J.: Human impacts on atmospheric chemisty, Ann. Rev. Earth Planet. Sci., 29, 17–45, 2001. 9397

Dunkerton, T.: Quasi-biennial and subbiennial variations of stratospheric trace constituents derived from HALOE observations, J. Atmos. Sci., 58, 7–25, 2001. 9395, 9396

Engel, A., Möbius, T., Haase, H.-P., Bönisch, H., Wetter, T., Schmidt, U., Levin, I., Reddmann, T., Oelhaf, H., Wetzel, G., Grunow, K., Huret, N., and Pirre, M.: On the observation of mesospheric air inside the arctic stratospheric polar vortex in early 2003, Atmos. Chem. Phys., 6, 267–282, 2006. 9398

ESA: MIPAS product handbook, European Space Agency, ESRIN, Frascati, Italy, available from http://www.envisat.esa.int/dataproducts, 2004. 9391

Farman, J. C., Gardiner, B. G., and Shanklin, J. D.: Large losses of total ozone in Antarctica reveal seasonal ClOx/NOx interaction, Nature, 315, 207–210, 1985. 9391, 9397

Fischer, H. and Oelhaf, H.: Remote sensing of vertical profiles of atmospheric trace constituents with MIPAS limb-emission spectrometers, Appl. Opt., 35, 2787–2796, 1996. 9391

Fonteyn, D., Lahoz, W., Geer, A., Dethof, A., Wargan, K., Stajner, I., Pawson, S., Rood, R., Bonjean, S., Chabrillat, S., Daerden, F., and Errera, Q.: MIPAS ozone assimilation, in Proceedings of the Second Workshop on the Atmospheric Chemistry Validation of ENVISAT (ACVE-2), European Space Agency, 2004. 9392

Geer, A. J., Lahoz, W. A., Bekki, S., Bormann, N., Errera, Q., Eskes, H. J., Fonteyn, D., Jackson, D. R., Juckes, M. N., Massart, S., Peuch, V.-H., Rharmili, S., and Segers, A.: The ASSET intercomparison of ozone analyses: method and first results, Atmos. Chem. Dyn. Discuss., 6, 4495–4577, 2006. 9391, 9397, 9402

Glatthor, N., Von Clarmann, T., Fischer, H., Funke, B., Grabowski, U., Hopfner, M., Kellmann, S., Kiefer, M., Linden, A., Milz, M., Steck, T., Stiller, G., Tsidu, G., and Wang, D.: Mixing processes during the antarctic vortex split in September–October 2002 as inferred from source gas and ozone distributions from ENVISAT-MIPAS, J. Atmos. Sci., 62, 787–800, 2005. 9391

Hannegan, B., Olsen, S., Prather, M., Zhu, X., Rind, and Lerner, J.: The dry stratosphere: a limit on cometary influx, Geophys. Res. Lett., 25, 1649–1652, 1998. 9402

Harries, J., Ruth, S., and Russell, J.: On the distribution of mesospheric molecular hydrogen inferred from HALOE measurements of H2O and CH4, Geophys. Res. Lett., 23, 297–300, 1996. 9401, 9403

Haynes, P. H., McIntyre, M. E., Shepherd, T. G., Marks, C. J., and Shine, K. P.: On the "Downward Control" of Extratropical Diabatic Circulations by Eddy-Induced Mean Zonal Forces, J. Atmos. Sci., 48, 651–678, 1991. 9398

Juckes, M.: Evaluation of MIPAS ozone fields assimilated using a new algorithm constrained by isentropic tracer advection, Atmos. Chem. Dyn., 6, 1549–1565, 2006. 9391

Lumpe, J. D., Fromm, M., Hoppel, K., Bevilacqua, R. M., Randall, C. E., Browell, E. V., Grant, W. B., McGee, T., Burris, J., Twigg, L., Richard, E. C., Toon, G. C., Sen, B., Boesch, H., Fitzenberger, R., and Pfeilsticker, K.: Comparison of POAM III ozone measurements with correlative aircraft and balloon data during SOLVE, J. Geophys. Res., 108(D5), 8316, doi:10.1029/2001JD000472 [2002], 2003. 9393

Mote, P., Rosenlof, K., Mcintyre, M., Carr, E., Gille, J., Holton, J., Kinnersley, J., Pumphrey, H., Russell, J., and Waters, J.: An atmospheric tape recorder: the imprint of tropical tropopause temperatures on stratospheric water vapor, J. Geophys. Res (D), 101, 3989–4006, 1996. 9396

Nassar, R., Bernath, P., Boone, C., Manney, G., Mcleod, S., Rinsland, C., Skelton, R., and Walker, K.: Stratospheric abundances of water and methane based on ACE-FTS measurements, Geophys. Res. Lett., 32, L15S04, doi:10.1029/2005GL022383, 2005. 9401

Pierce, R. B., Al-Saadi, J., Fairlie, T. D., Natarajan, M., Harvey, V. L., Grose, W. L., Russell, J. M., Bevilacqua, R., Eckermann, S. D., Fahey, D., Popp, P., Richard, E., Stimpfle, R., Toon, G. C., Webster, C. R., and Elkins, J.: Large-scale chemical evolution of the arctic vortex during the 1999–2000 winter: HALOE/POAM3 lagrangian photochemical modelling for the SAGE III ozone loss and validation experiment (SOLVE) campaign, J. Geophys. Res., 108(D5), 8317, doi:10.1029/2001JD001063 [2002], 2003. 9393

Planet, W. G., Miller, A. J., Horvath, K., Nagatani, R., Flynn, L., Hilsenrath, E., Kondragunta, S., Cebula, R. P., and DeLand, M. T.: Total ozone determinations from NOAA operational SBUV/2 observations: an update, J. Geophys. Res., 106(D15), 17 471–17 478, 2001. 9393

Randel, W., Wu, F., Russell, J., Roche, A., and Waters, J.: Seasonal cycles and QBO variations in stratospheric CH4 and H2O observed in UARS HALOE data, J. Atmos. Sci., 55, 163–185, 1998. 9395, 9397

Rex, M., Salawitch, R., Toon, G., Sen, B., Margitan, J., Osterman, G., Blavier, J., Gao, R., Donnelly, S., Keim, E., Neuman, J., Fahey, D., Webster, C., Scott, D., Herman, R., May, R., Moyer, E., Gunson, M., Irion, F., Chang, A., Rinsland, C., and Bui, T.: Subsidence, mixing, and denitrification of arctic polar vortex air measured during polaris, J. Geophys. Res (D), 104, 26 611–26 623, 1999. 9398

Rind, D. and Lonergan, P.: Modeled impacts of stratospheric ozone and water-vapor perturbations with implications for high-speed civil transport aircraft, J. Geophys. Res (D), 100, 7381–7396, 1995. 9390

Rosenfield, J. E., Newman, P. A., and Schoeberl, M. R.: Computations of diabatic descent in the stratospheric polar vortex, J. Geophys. Res., 99(D8), 16 677–16 690, doi:10.1029/94JD01156, 1994. 9398

Rosenlof, K., Oltmans, S., Kley, D., Russell, J., Chiou, E., Chu, W., Johnson, D., Kelly, K., Michelsen, H., Nedoluha, G., Remsberg, E., Toon, G., and McCormick, M.: Stratospheric water vapor increases over the past half-century, Geophys. Res. Lett., 28(7), 1195–1198, 2001. 9390

Scott, R. and Haynes, P.: The seasonal cycle of planetary waves in the winter stratosphere, J. Atmos. Sci., 59, 803–822, 2002. 9397

Shindell, D.: Climate and ozone response to increased stratospheric water vapor, Geophys.

Res. Lett., 28, 1551–1554, 2001. 9390
Shine, K.: The greenhouse effect and stratosheric change, in: NATO ASI 18, edited by: Chanin, M.-L., pp. 285–300, Springer-Verlag, Berlin, 1993. 9391
Solomon, S., Portmann, R. W., Sasaki, T., Hofmann, D. J., and Thompson, D. W. J.: Four decades of ozonesonde measurements over antarctica, J. Geophys. Res (D), 110, D21311, doi:10.1029/2005JD005917, 2005. 9391
Thomason, L. W. and Taha, G.: SAGE III aerosol extinction measurements: initial results, Geophys. Res. Lett., 30, 33-1–33-4, doi:10.1029/2003GL017317, 2003. 9393
Tsidu, G. M., Kiefer, M., von Clarmann, T., Fischer, H., Funke, B., Grabowski, U., Hase, F., Höpfner, M., López-Puertas, M., and Stiller, G. P.: Validation of MIPAS/ENVISAT level-1b data products, edited by: Huang, H.-L., Lu, D., and Sasano, Y., Optical Remote Sensing of the Atmosphere and Clouds III, Proc. of SPIE, 4891, 483–496, 2003. 9391
von Savigny, C., Haley, C. S., Sioris, C. E., McDade, I. C., Llewellyn, E. J., Degenstein, D., Evans, W. F. J., Gattinger, R. L., Griffoen, E., Lloyd, N., McConnell, J. C., McLinden, C. A., Murtagh, D. P., Solheim, B., and Strong, K.: Stratospheric ozone profiles retrieved from limb scattered sunlight radiance spectra measured by the OSIRIS instrument on the ODIN satellite, Geophys. Res. Lett., 30, 1755–1758, doi:10.1029/2002GL016401, 2003. 9393

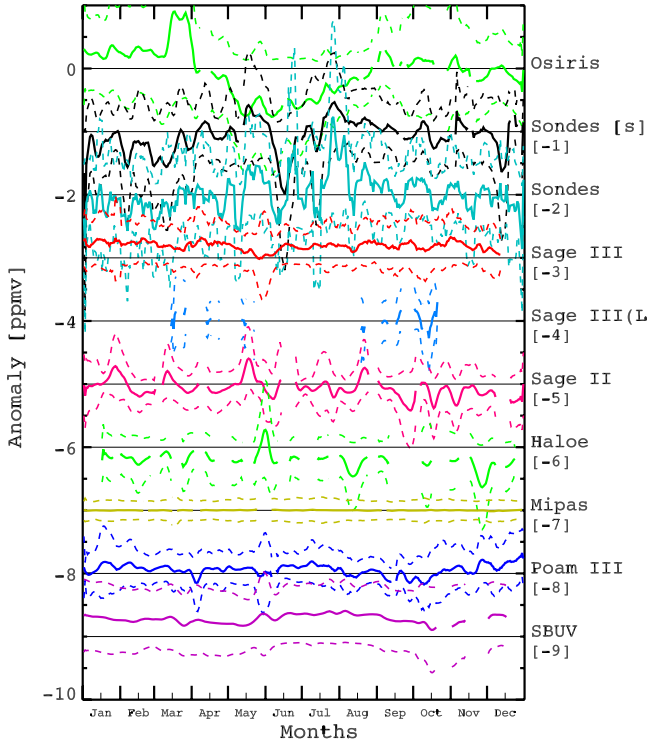

Fig. 1. Time sequence of observation minus assimilation on the 850K isentropic surface. The mean for each day, taken over all observations on that day, is plotted as solid lines, with dashed lines at plus/minus one standard deviation. SAGE III [L] is the data from the lunar occultation mode of SAGE III. Sondes [S] is data from the WOUDC ozone sondes which has been vertically smoothed with a 2 km running mean. Offsets (in square brackets below the name of each instrument) have been added to separate the plots.

ACPD
6, 9389–9429, 2006

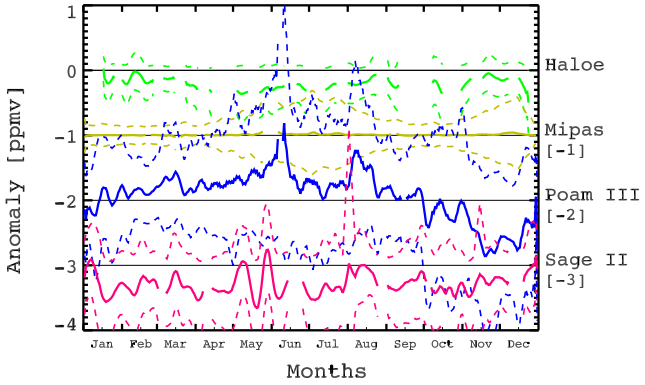

Fig. 2. As Fig. 1, except for water vapour.

ACPD
6, 9389–9429, 2006

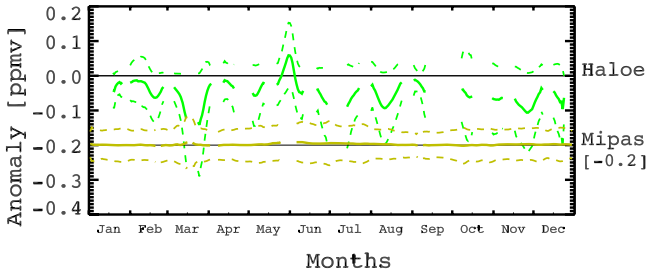

Fig. 3. As Fig. 1, except for methane.

ACPD
6, 9389–9429, 2006

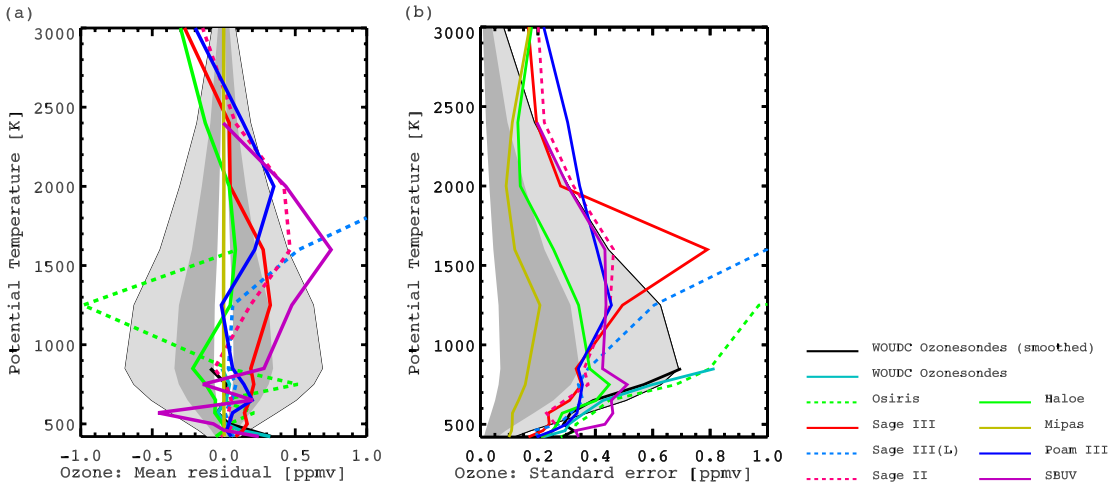

Fig. 4. Vertical profile of ozone **(a)** mean error (observation minus assimilation) and **(b)** standard deviation (root mean square differences after subtraction of the mean) against potential temperature. The shading shows the 1–5% (dark) and 5–10% (light) range, compared with the mean assimilation profile.

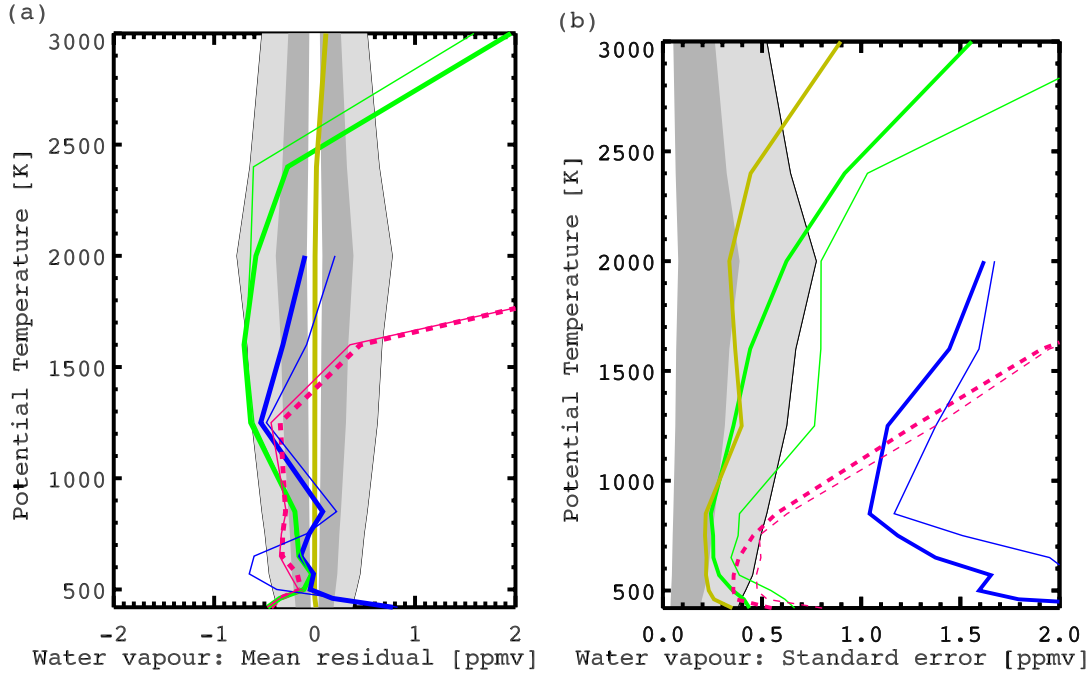

Fig. 5. As for Fig. 4, except for water vapour, and additional thin lines show nearest-neighbour validation profiles. These are the mean difference and standard error between MIPAS level 2 profiles and those of the other instruments taken over all pairs occurring within 2.5 degrees and 6 h of each other.

ACPD
6, 9389–9429, 2006

EGU

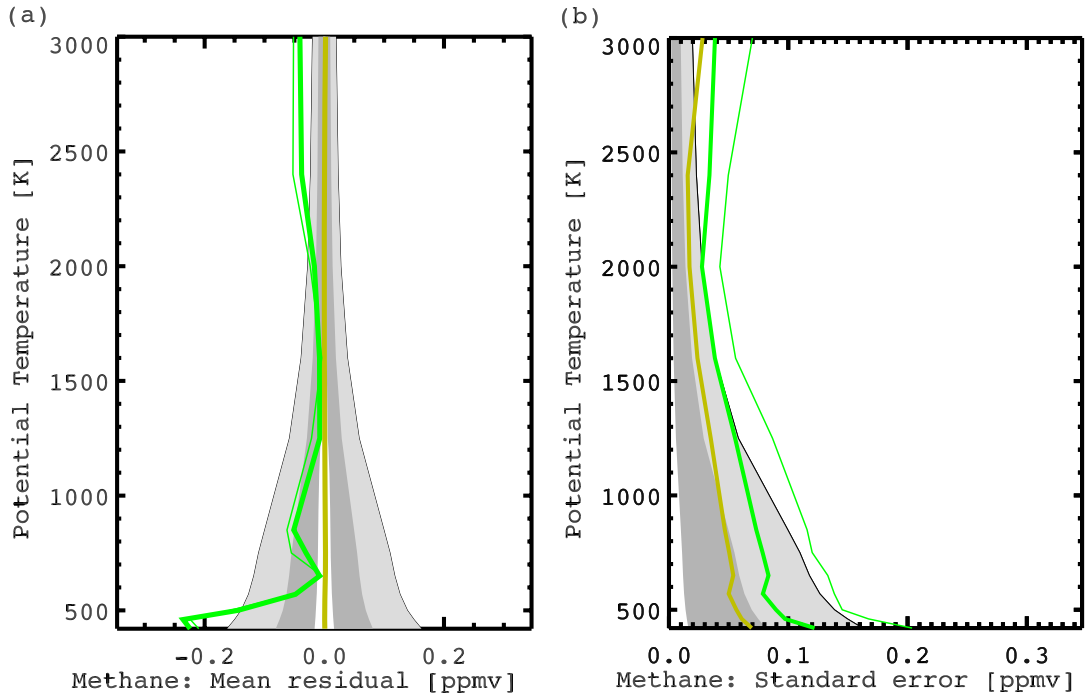

Fig. 6. As for Fig. 5, except for methane.

ACPD
6, 9389–9429, 2006

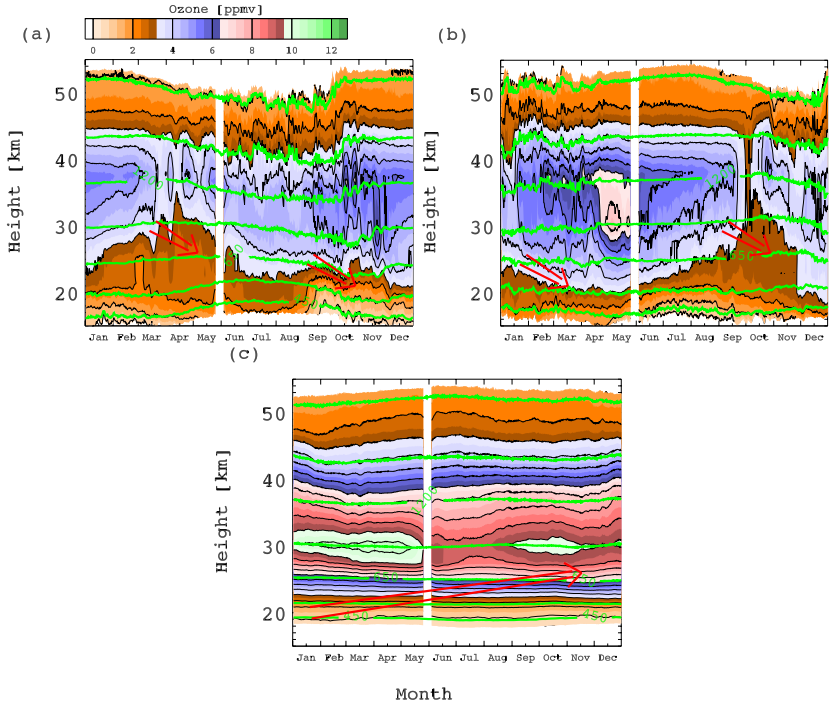

Fig. 7. Time height sections of analyses averaged over equivalent latitude bands. The fields are: ozone **(a, b, c)**, water vapour **(d, e, f)** and methane **(g, h, i)**. The equivalent latitude bands are: South of 80 S (a, d, g), north of 80 N (b, e, h) and 5 S to 5 N (c, f, i). For each species the colour scale is given at the top of the column. The contour intervals are: 0.8 ppmv (ozone), 0.4 ppmv (water vapour) and 0.2 ppmv (methane). Isentropes are contoured in green, at 450, 520, 650, 850, 1200, 1650 and 2300 K. In (a, b, d, e, g, h) red arrows slope downwards at a rate of 100 m/day. In (c, f, i) red arrows slope upwards at a rate of 20 m/day.

ACPD
6, 9389–9429, 2006

EGU

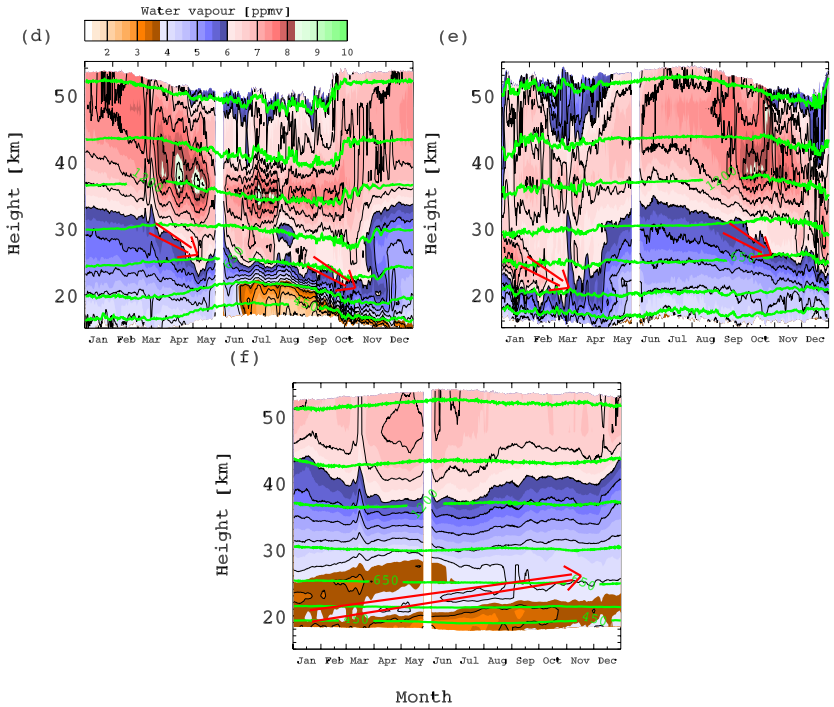

Fig. 7. Continued.

ACPD
6, 9389–9429, 2006

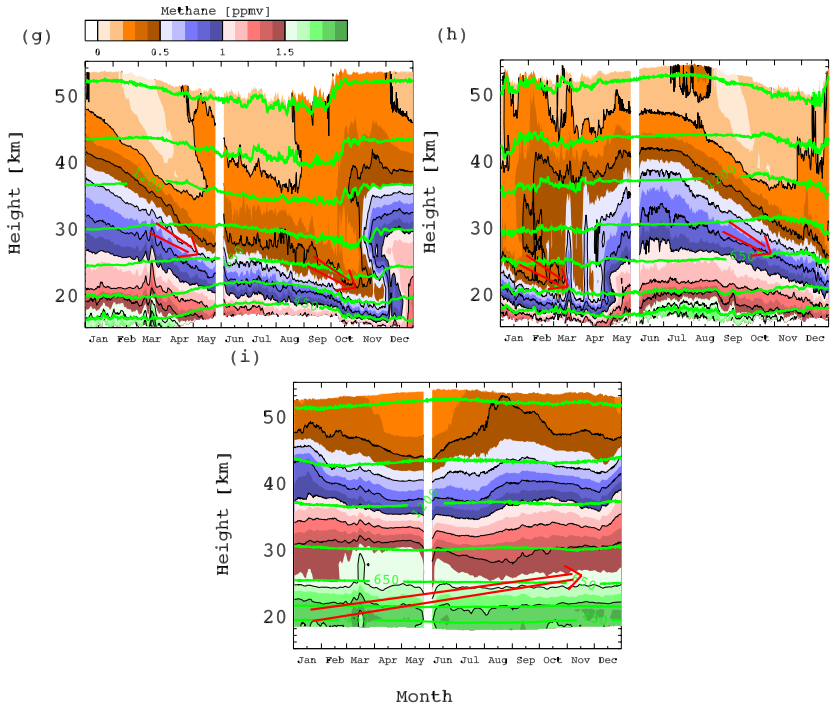

Fig. 7. Continued.

ACPD
6, 9389–9429, 2006

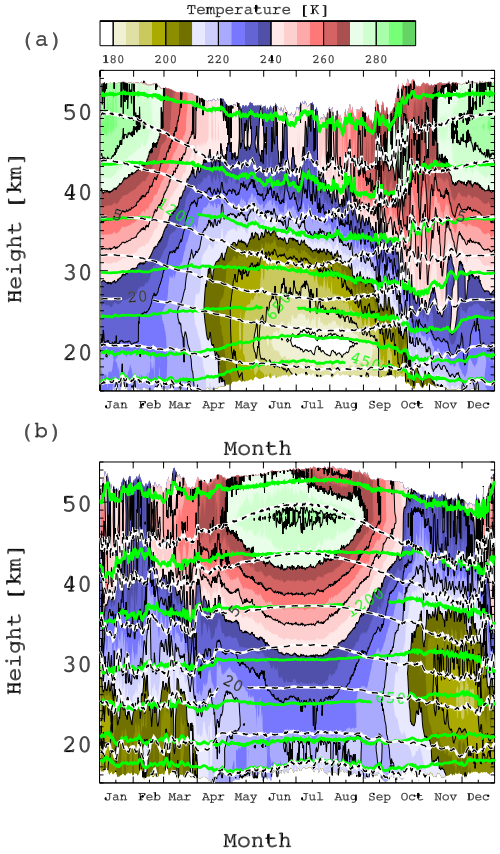

Fig. 8. As Fig. 7, but showing temperature. Pressure contours are shown (black dashes on white) for 1, 2, 5, 10, 20, 50, 100 hPa. **(a)** South, **(b)** North.

ACPD
6, 9389–9429, 2006

EGU

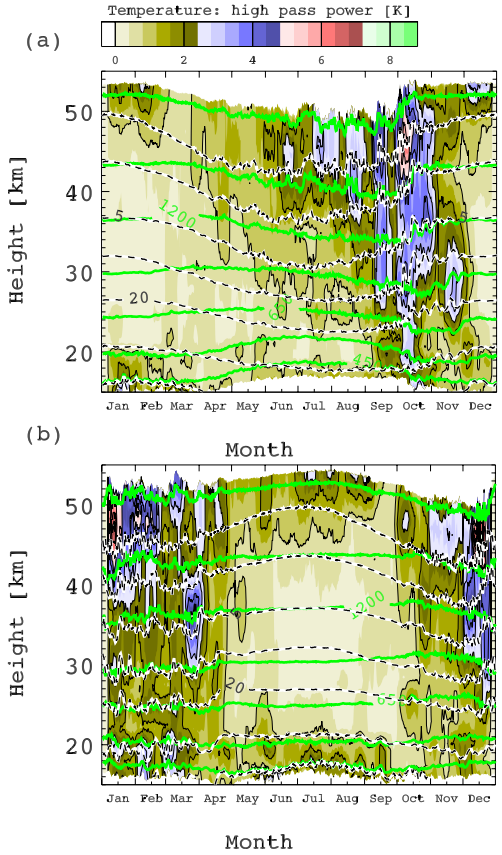

Fig. 9. As Fig. 8, but showing intensity of high pass temperature variability ($\sqrt{LP[HP[T]^2]}$, where the operator LP is a low pass filter (a 10 day running mean) and HP is a high pass filter, taken as the residual from LP).

ACPD
6, 9389–9429, 2006

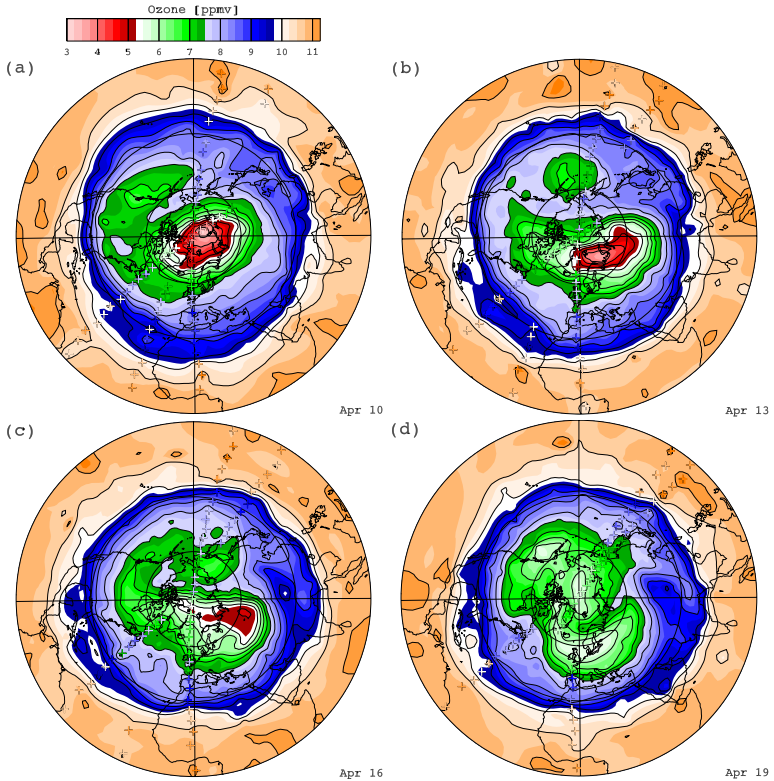

Fig. 10. Ozone (**a–d**, contour interval 0.5 ppmv), water vapour (**e–h**, contour interval 0.2 ppmv), and methane (**i–l**, contour interval 0.1 ppmv), on 10 to 19 April 2003 (in steps of 3 days, starting at the top), on the 850 K isentropic surface. Ozone, water vapour and methane are assimilated from MIPAS level 2 data as described in the text. Each analysis is valid at 00:00 GMT. The crosses indicate MIPAS profiles taken within 2 h of this time, and are coloured using the same scale as the fields.

ACPD
6, 9389–9429, 2006

EGU

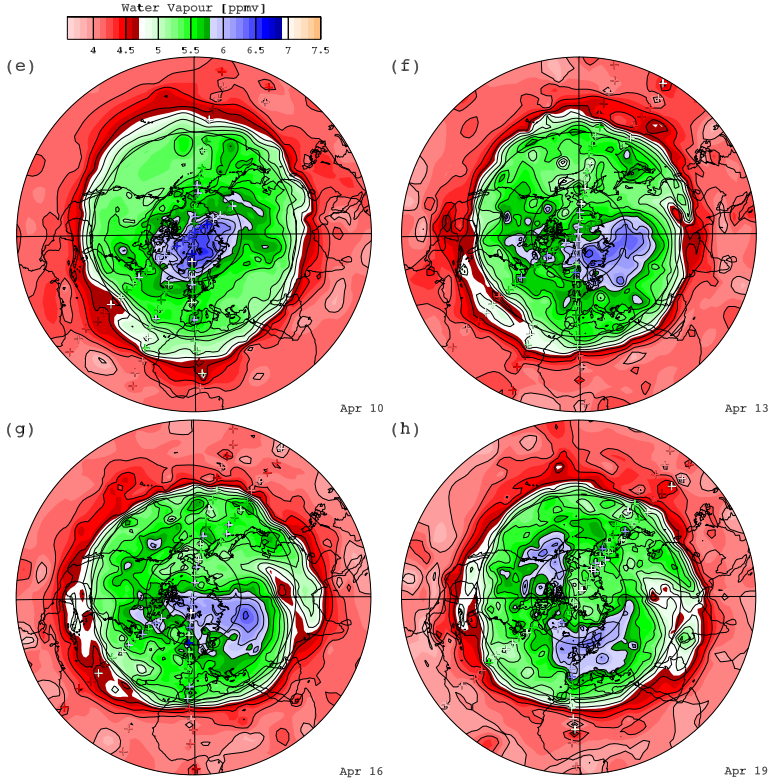

Fig. 10. Continued.

ACPD
6, 9389–9429, 2006

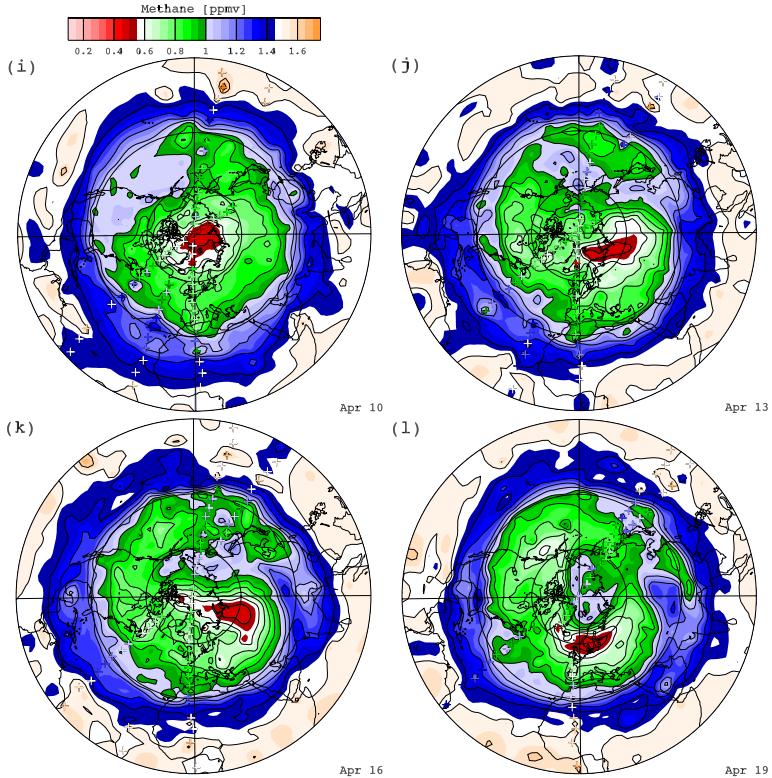

Fig. 10. Continued.

ACPD
6, 9389–9429, 2006

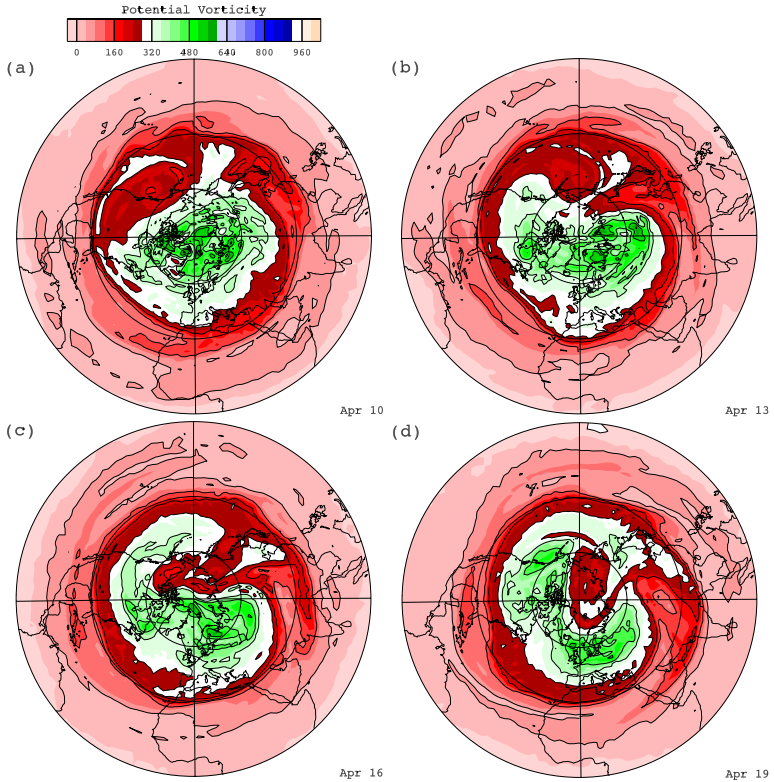

Fig. 11. As Fig. 10, except showing Ertel potential vorticity from the ECMWF operational analyses, contour interval $8\times10^{-5}\,\mathrm{K\,kg^{-1}\,s^{-1}}$. The colour scale (top) is labeled in units of $10^{-6}\,\mathrm{K\,kg^{-1}\,s^{-1}}$.

ACPD
6, 9389–9429, 2006

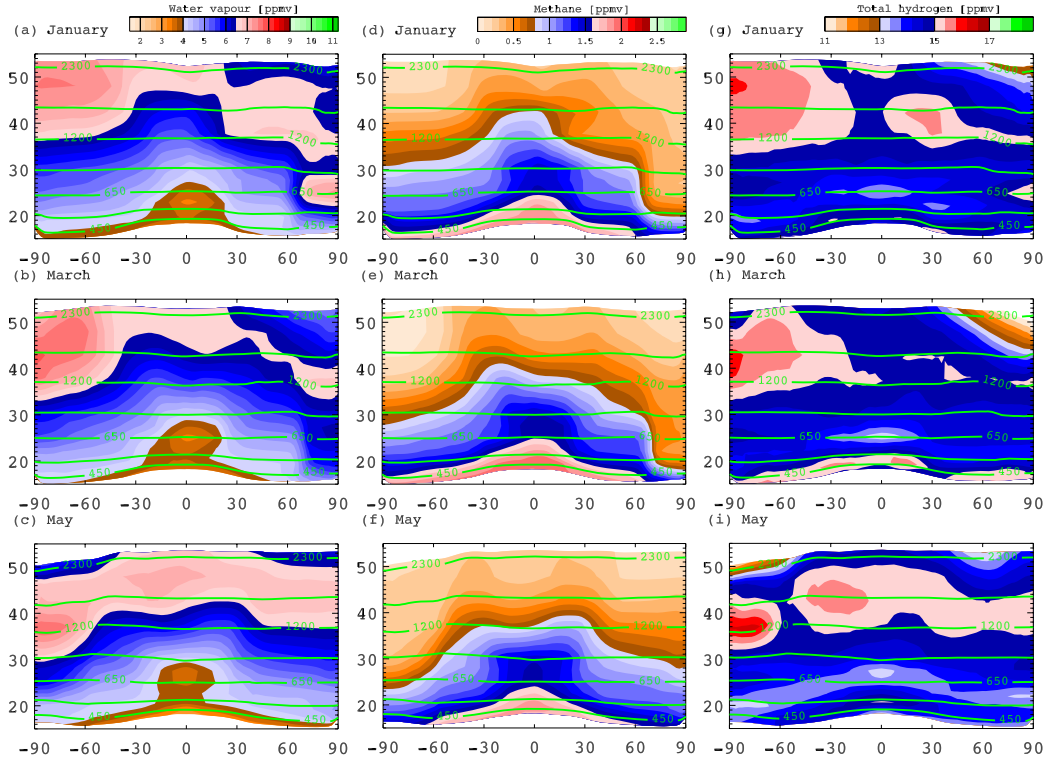

Fig. 12. Monthly, equivalent latitude means of water vapour, methane and total observed hydrogen (H_{TO}) for January, March and May. Fields shown are water vapour **(a, b, c)**, methane **(d, e, f)** and H_{TO} **(g, h, i)**. Green contours show the heights of isentropic surfaces (these figures are generated from data on isentropic).

ACPD
6, 9389–9429, 2006

EGU

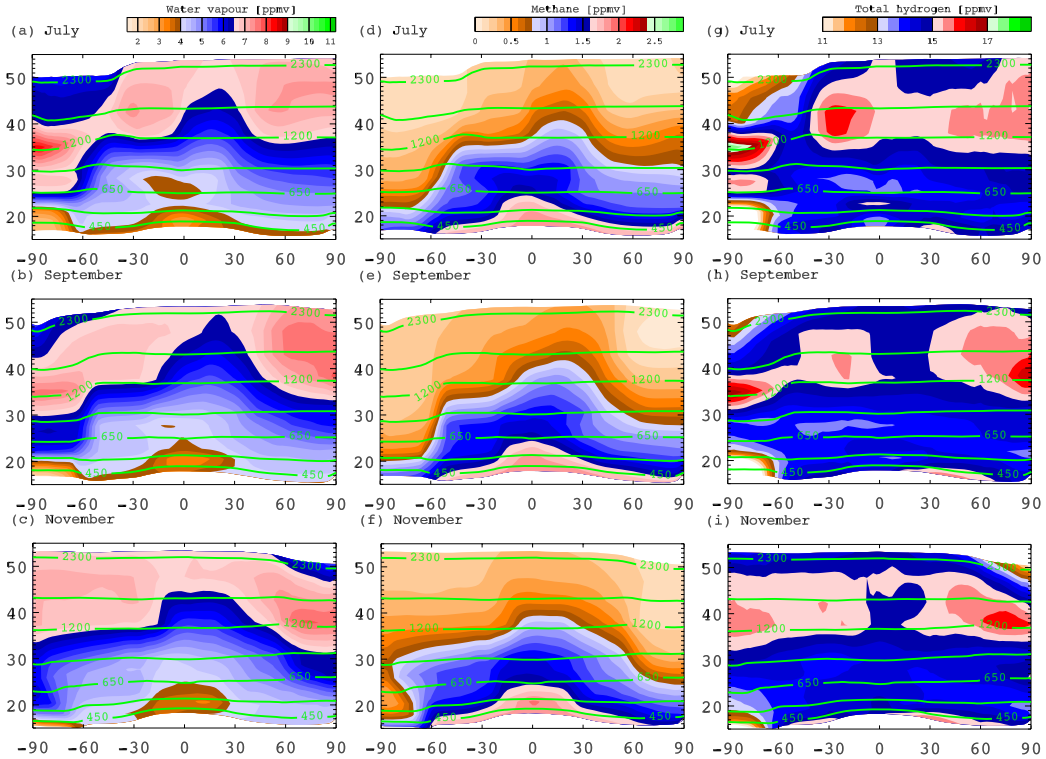

Fig. 13. As for Fig. 12, except for July, September, November.

ACPD
6, 9389–9429, 2006

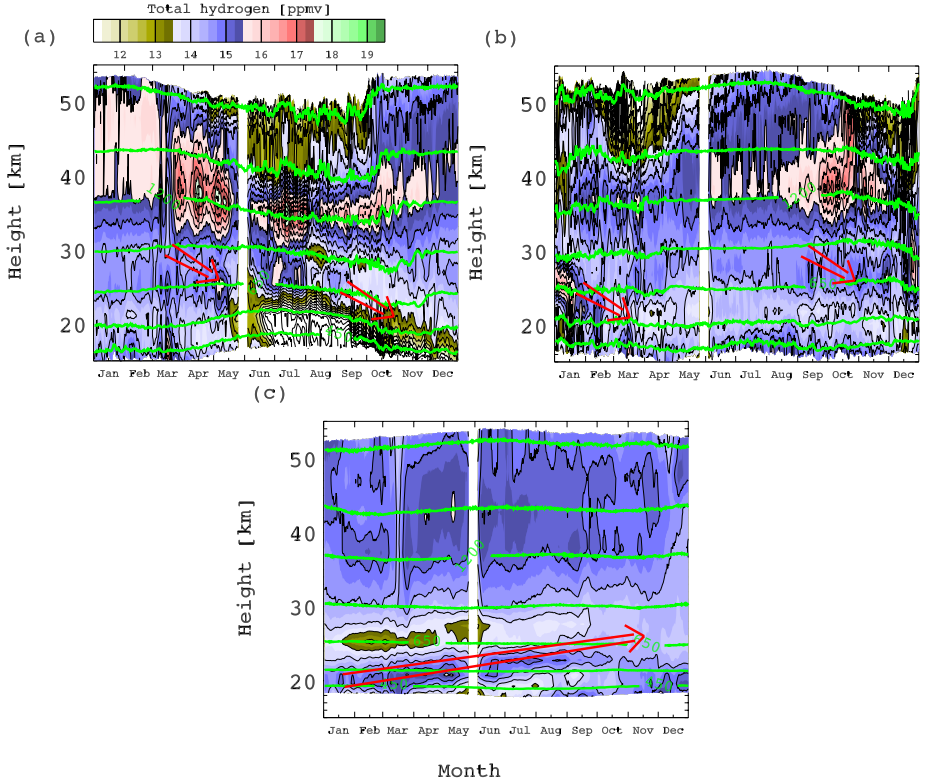

Fig. 14. As Fig. 7, but showing total observed hydrogen.

ACPD
6, 9389–9429, 2006

EGU

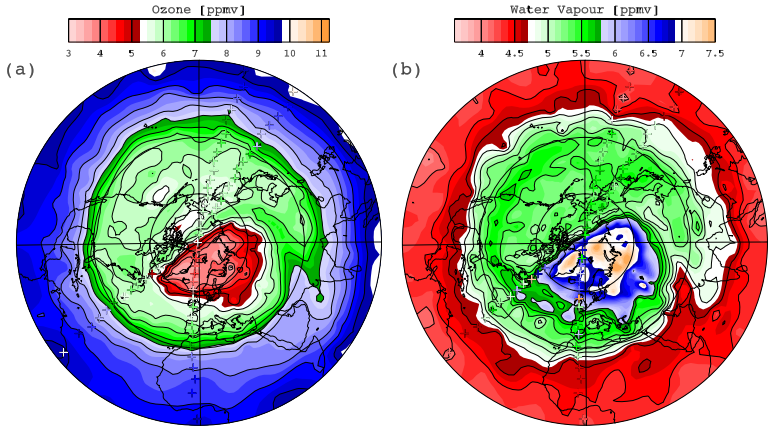

Fig. 15. Ozone, water vapour, methane, Ertel potential vorticity and H_{TO} on 20 December 2003. All are northern polar stereographic plots on the 850 K isentropic surface.

ACPD
6, 9389–9429, 2006

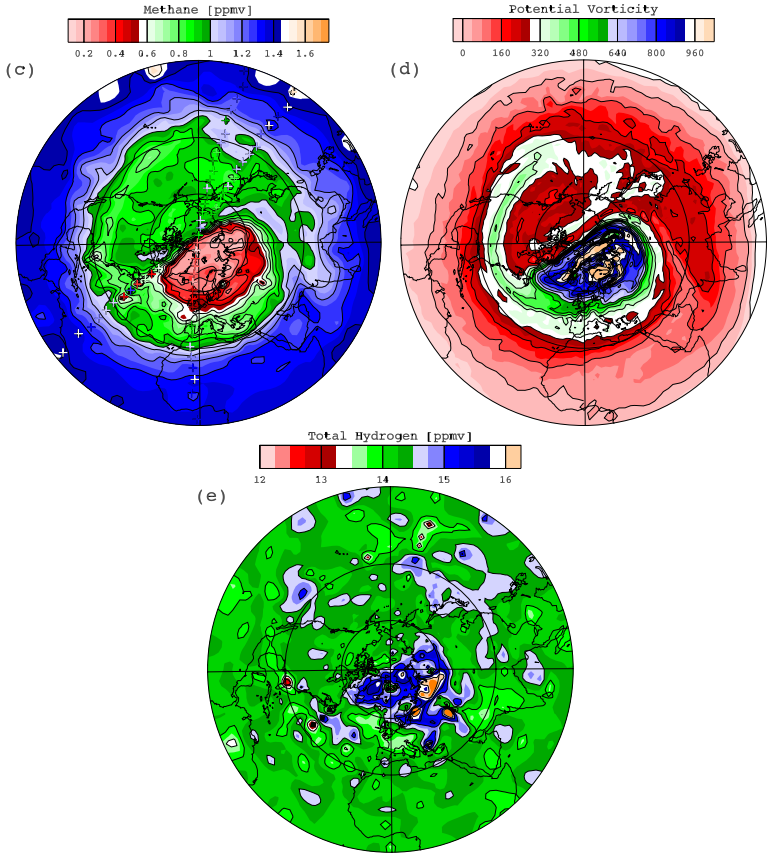

Fig. 15. Continued.

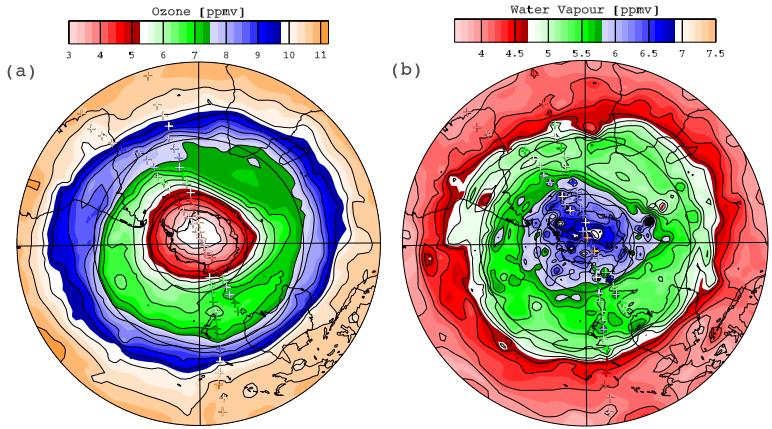

Fig. 16. As Fig. 15, except southern polar stereographic plots for 20 April 2003.

ACPD
6, 9389–9429, 2006

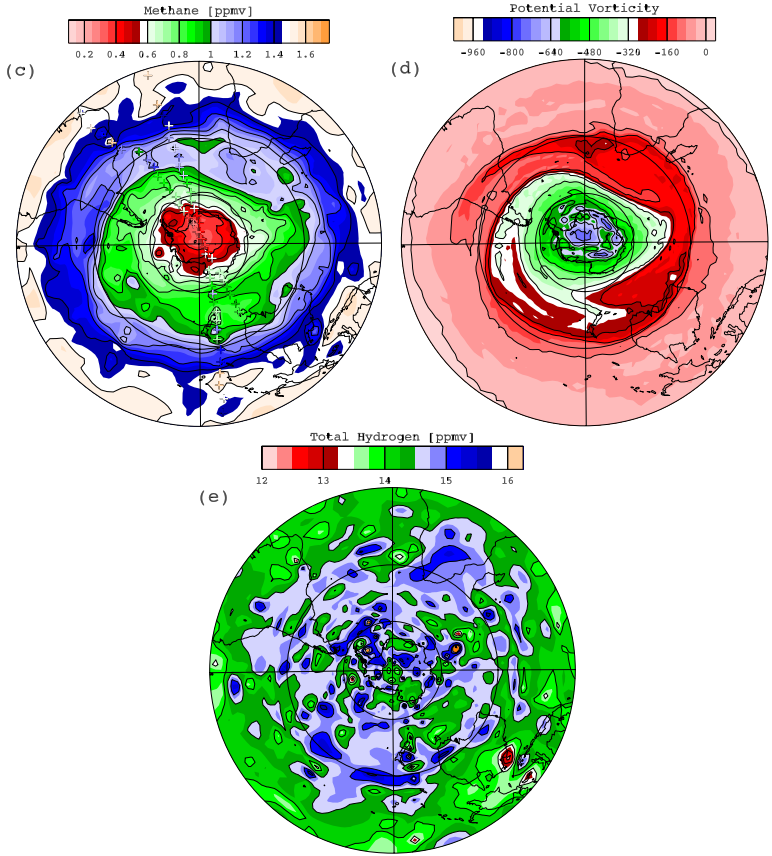

Fig. 16. Continued.

ACPD
6, 9389–9429, 2006

EGU